Z. Hou, Y. Geng, S. Huang
Minimum Residual Vibrations for Flexible Satellites with Frequency Uncertainty
IEEE Transactions on Aerospace and Electronic Systems, Vol. 54, N. 2, 2018, p. 1029-1038
doi:10.1109/TAES.2017.2773321

Minimum Residual Vibrations for Flexible Satellites with Frequency Uncertainty

Zhili Hou, Yunhai Geng, and Simeng Huang

***Abstract*—The resonant frequencies will be excited if satellites perform a rapidly maneuver, which will increase the vibration settling time. In order to reduce the maneuver time and the residual vibration after maneuver, a set of shaped angular acceleration profiles are presented, and their analytical solutions are derived by minimizing the time integral of the squared magnitude of the difference between angular acceleration and its mean value subject to that the magnitude of the residual vibrations at several frequencies surrounding the natural frequency are zero. Then, suitable frequency points, where the residual vibrations are constrained to be zero, are chosen to minimize the acceleration time subject to both the residual vibration magnitude limit and the angular acceleration magnitude limit. Finally, three sets of simulations are presented to demonstrate that the shaped angular acceleration profiles can reduce the residual vibration under the frequency uncertainty.**

***Index Terms*—Flexible spacecraft, vibration reduction, frequency uncertainty, trajectory planning.**

I. Introduction

If a satellite performs a rapid maneuver, vibrations in the flexible appendages (solar panels or flexible antennae) will be excited. These vibrations are particularly detrimental at the end of the maneuver, where precision is usually demanded. Some vibration reduction methods have been developed to reduce residual vibrations at the end of maneuvers.

Input shaping[1], a class of widely-used methods, is a command generation technique to reduce residual vibrations that surround natural frequencies and works such as a notch filter that cancels out the decaying sinusoidal response. Singer and Seering[2] presented the ZV (zero vibration) shaper to eliminate residual vibrations at natural frequencies. However, the ZV shaper is limited to applications where the natural frequencies do not change significantly. To overcome this weakness, Singer and Seering[2] presented the ZVD (zero vibration derivative) shaper to improve the robustness for frequency changes. The ZVD shaper was derived by forcing the derivative of the residual vibration with respect to frequency to equal zero at the natural frequencies. Furthermore, Singhose[3–5] presented an approach named the EI (extra insensitive) shaper, which provides extra robustness without increasing the shaper duration when compared with the ZVD shaper. Singhose, Seering and Singer[6] then presented a more general method called the SI (specified insensitive) shaper to suppress a specified range of frequencies. In addition, a summary and comparison of input shaping methods were presented[7, 8].

Input smoothing is another class of effective method was methods that was developed by shaping the input command as a type of a smooth profile to reduce residual vibrations. Meckl[9] developed optimal s-curve motion profiles by minimizing the ramp-up time to achieve fast motions with minimum vibrations. Junkins[10] used the s-curve as input profiles to develop a near minimum time control law for a flexible satellite. The parameters of the s-curve profiles were chosen by minimizing the combination of vibration energy and maneuver time. Swigert[11] developed a set of smooth input torques constructed from a series of specified trigonometric functions. The coefficients of the trigonometric functions were calculated by minimizing the weighted combination of the squared magnitude of the input torque and the sensitivity of the residual vibration to model errors. Meckl[12, 13] presented two types of force profiles constructed from a versine(1-cosine) function and ramped sinusoid function. The excitation in a range of frequencies surrounding the system natural frequency was then minimized to obtain the coefficients. Xie X[14] designed an optimal smooth filter with high robustness at high frequencies compared with a ZVDDD input shaper.

The input smoothing method has an inherent advantage over the input shaping method because it can provide smooth input profiles that are conducive to trajectory tracking control. However, the smooth input profiles were often chosen as certain types of functions such as an s-curve, the summation of versine functions, and the summation of ramped sinusoid functions, which incapable of representing an arbitrary function. In this paper, the input(angular acceleration) profiles are allowed to be any reasonable function, and the analysis expression of this input profile then is derived by minimizing the time integral of the squared magnitude of the difference between the angular acceleration and its mean value, subject to the constraints that the magnitudes of the residual vibrations at several frequency points surrounding the natural frequency are zero. Then, suitable positions of the zero vibration frequencies are chosen to keep both the angular acceleration and residual vibration within acceptable bounds and at the same time, to minimize the acceleration time. In addition, the smooth input profile developed in this paper can also be used in the system where the damping is not zero.

Zhili Hou is with 805 Research Institute of Shanghai Academy of Spaceflight Technology, China e-mail: (hzl1334123@163.com).
Yunhai Geng is with Harbin Institute of Technology.
Simeng Huang is with Politecnico di Milano.

The remainder of this paper contains three main sections. Section II develops the mathematical expression of the angular acceleration and residual vibrations under the assumption that the control error is small. Section III develops the analytical expression for the optimal angular acceleration profiles to minimize the residual vibration. Section IV discusses a set of simulations to verify that the developed angular acceleration profiles are valid to suppress residual vibrations under frequency uncertainty.

II. Relationship between Angular Acceleration Profiles and Residual Vibrations

This section first introduces the dynamic equations for a flexible satellite and attitude tracking controller, presents a derivation of the response of the residual vibration to an arbitrary input, and finally presents an evaluation index to measure the effectiveness of the vibration suppression.

A. Satellite Dynamic Equations and Kinematics

The attitude dynamics of a flexible satellite are given by

$$\left\{ \begin{array}{l} \boldsymbol{I}\dot{\boldsymbol{\omega}} + \boldsymbol{\omega} \times \boldsymbol{I}\boldsymbol{\omega} + \boldsymbol{\omega} \times \boldsymbol{h}_c + \boldsymbol{B}\ddot{\boldsymbol{\eta}} = \boldsymbol{T}_c \\ \ddot{\boldsymbol{\eta}} + 2\xi\boldsymbol{\Omega}\dot{\boldsymbol{\eta}} + \boldsymbol{\Omega}^2\boldsymbol{\eta} + \boldsymbol{B}^{\mathrm{T}}\dot{\boldsymbol{\omega}} = \boldsymbol{0} \end{array} \right. \tag{1}$$

where $\boldsymbol{I}$ is the inertia matrix, $\boldsymbol{\omega} = [\omega_x \quad \omega_y \quad \omega_z]^{\mathrm{T}}$ is the body angular velocity relative to the inertial reference frame, $\boldsymbol{h}_c$ is the total angular momentum of the flywheel, $\boldsymbol{T}_c$ is the control torque input vector, $\boldsymbol{\eta} = [\eta_1 \quad \eta_2 \quad \cdots \quad \eta_m]^{\mathrm{T}}$ is a generalized coordinate vector, m is the number of modes, ξ is the modal damping ratio, $\boldsymbol{\Omega}$ is a diagonal matrix with entries Ω_j which is the j^{th} natural frequency, $\boldsymbol{\Omega}^2$ is a diagonal frequency matrix with entries ${\Omega_j}^2$, and $\boldsymbol{B}$ is the coupling matrix between the rigid body and appendages.

The kinematics as described by quaternions are

$$\dot{\boldsymbol{q}}_v = -\frac{1}{2}\boldsymbol{\omega} \times \boldsymbol{q}_v + \frac{1}{2}q_0\boldsymbol{\omega}, \text{ and} \tag{2}$$

$$\dot{q}_0 = -\frac{1}{2}\boldsymbol{\omega}^{\mathrm{T}}\boldsymbol{q}_v \tag{3}$$

where $\boldsymbol{q}_v = [q_1 \quad q_2 \quad q_3]^{\mathrm{T}}$ is the quaternion vector of $\boldsymbol{q} = [q_0 \quad q_1 \quad q_2 \quad q_3]^{\mathrm{T}}$, which is the quaternion relative to the inertial reference frame.

B. Simplification of the Vibration Equation

Assume that the reference trajectory is scheduled as an eigenaxis rotation. A PD controller is then given by

$$\boldsymbol{T}_c = \boldsymbol{I}\left(-k_p\boldsymbol{q}_{ev} - k_d\boldsymbol{\omega}_e\right) + \boldsymbol{T}_r\left(t\right) + \boldsymbol{\omega} \times \left(\boldsymbol{I}\boldsymbol{\omega} + \boldsymbol{h}_c\right) \tag{4}$$

where $\boldsymbol{q}_{ev} = [q_{e1} \quad q_{e2} \quad q_{e3}]^{\mathrm{T}}$ is the vector part of $\boldsymbol{q}_e = [q_{e0} \quad q_{e1} \quad q_{e2} \quad q_{e3}]^{\mathrm{T}}$ which represents the error quaternion, $\boldsymbol{\omega}_e$ is the error angular velocity, and $\boldsymbol{T}_r\left(t\right)$ is the reference torque, which is expressed as

$$\boldsymbol{T}_r\left(t\right) = \boldsymbol{I}\boldsymbol{e}a_r\left(t\right) \tag{5}$$

where $a_r(t)$ is the reference angular acceleration to be scheduled, and $\boldsymbol{e}$ is the fixed eigenaxis. $\boldsymbol{q}_{ev}$ and $\boldsymbol{\omega}_e$ can be obtained according to the equations

$$\boldsymbol{\omega}_e = \boldsymbol{\omega} - \boldsymbol{\omega}_r\left(t\right), \text{ and} \tag{6}$$

$$\boldsymbol{q}_{ev} = -q_0\boldsymbol{q}_{rv}\left(t\right) + q_{r0}\left(t\right)\boldsymbol{q}_v - \boldsymbol{q}_{rv}\left(t\right) \times \boldsymbol{q}_v \tag{7}$$

where $\boldsymbol{\omega}_r\left(t\right) = [\omega_{rx}\left(t\right) \quad \omega_{ry}\left(t\right) \quad \omega_{rz}\left(t\right)]^{\mathrm{T}}$ is the reference angular velocity, and the expressions for $q_{r0}\left(t\right)$ and $\boldsymbol{q}_{rv}\left(t\right)$ are

$$q_{r0}\left(t\right) = \cos\left(\frac{\Phi_r\left(t\right)}{2}\right), \quad \boldsymbol{q}_{rv}\left(t\right) = \boldsymbol{e}\sin\left(\frac{\Phi_r\left(t\right)}{2}\right) \tag{8}$$

where $\Phi_r\left(t\right)$ is the reference principal rotation angle. $\boldsymbol{\omega}_r\left(t\right)$ and $\Phi_r\left(t\right)$ can be obtained by integrating $a_r\left(t\right)$.

After substituting Eq. (4) and Eq. (5) into the first equation of Eq. (1), simplifying yields

$$\dot{\boldsymbol{\omega}} = -\boldsymbol{I}^{-1}\boldsymbol{B}\ddot{\boldsymbol{\eta}} - k_p\boldsymbol{q}_e - k_d\boldsymbol{\omega}_e + \boldsymbol{e}a_r\left(t\right) \tag{9}$$

If the satellite attitude can track the reference trajectory well, the actual angular acceleration $\dot{\boldsymbol{\omega}}$ is approximately equal to the reference angular acceleration $\boldsymbol{e}a_r\left(t\right)$. The second equation of Eq. (1) then can be simplified to

$$\ddot{\boldsymbol{\eta}} + 2\xi\boldsymbol{\Omega}\dot{\boldsymbol{\eta}} + \boldsymbol{\Omega}^2\boldsymbol{\eta} = -\boldsymbol{B}^{\mathrm{T}}\boldsymbol{e}a_r\left(t\right) \tag{10}$$

where

$$\boldsymbol{D} = -\boldsymbol{B}^{\mathrm{T}}\boldsymbol{e} \tag{11}$$

Remark: Using the approximation $\dot{\boldsymbol{\omega}} \approx \boldsymbol{e}a_r\left(t\right)$ will lead to a small difference between the actual and ideal frequencies. However, this difference can be considered to be a part of the frequency uncertainty that will be considered in the derivation of the optimal angular acceleration profiles.

C. Expression of the Residual Vibrations

With an arbitrary input function $a_r\left(t\right)$, the residual vibration after a maneuver is expressed as

$$\eta_j\left(t\right) = \int_0^{t_f} a_r\left(\tau\right)\eta_{\delta j}\left(t-\tau\right)d\tau \tag{12}$$

where t_f is the maneuver time, and $\eta_{\delta j}\left(t\right)$ is the impulse response of the j^{th} modal vibration, whose expression is given by

$$\eta_{\delta j}\left(t\right) = \frac{D_j e^{-\kappa_j\xi t}\sin\left(\kappa_j\sqrt{1-\xi^2}t\right)}{\kappa_j\sqrt{1-\xi^2}} \tag{13}$$

where D_j is the jth element of $\boldsymbol{D}$.

The response of the j^{th} modal vibration with the input $a_r\left(t\right)$ can be written as Eq. (16). The expression for the maximum amplitude of residual vibration then can be written as Eq. (17). To measure the vibration suppression effectiveness, define the *Residual Vibration Ratio* as

$$\upsilon = \frac{V\left(\kappa\right)}{\eta_{\mathrm{step}}\left(\kappa\right)} \tag{14}$$

where $V(\kappa)$ is the amplitude of the residual vibration at frequency κ, η_{step} is the maximum value of the step response of the vibration system shown in Eq. (10), where

$$\begin{aligned}\eta_j(t) &= D_j\int_0^{t_f} a(\tau)\,\eta_{\delta j}(t-\tau)d t\\ &= \frac{D_j e^{-\kappa_j\xi t}\sin\left(\kappa_j\sqrt{1-\xi^2}t\right)}{\kappa_j\sqrt{1-\xi^2}}\int_0^{t_f} a(\tau)\,e^{\kappa_j\xi\tau}\cos\left(\kappa_j\sqrt{1-\xi^2}\tau\right)d\tau\\ &-\frac{D_j e^{-\kappa_j\xi t}\cos\left(\kappa_j\sqrt{1-\xi^2}t\right)}{\kappa_j\sqrt{1-\xi^2}}\int_0^{t_f} a(\tau)\,e^{\kappa_j\xi\tau}\sin\left(\kappa_j\sqrt{1-\xi^2}\tau\right)d\tau\end{aligned} \tag{16}$$

$$V_j = \frac{D_j e^{-\kappa_j\xi t_f}\sqrt{\left(\int_0^{t_f} a(\tau)\,e^{\kappa_j\xi\tau}\cos\left(\kappa_j\sqrt{1-\xi^2}\tau\right)d\tau\right)^2+\left(\int_0^{t_f} a(\tau)\,e^{\kappa_j\xi\tau}\sin\left(\kappa_j\sqrt{1-\xi^2}\tau\right)d\tau\right)^2}}{\kappa_j\sqrt{1-\xi^2}} \tag{17}$$

$\xi = 0$, and the step amplitude is $a_{\max}$. The expression for η_{step} is

$$\eta_{\text{step}} = \frac{2D_j a_{\max}}{\kappa^2} \tag{15}$$

where $a_{\max}$ is the allowed maximum angular acceleration.

III. Development of the Optimal Angular Acceleration Profiles

The angular acceleration profiles to be developed are intended for angular velocity-limited system where the angular velocity profile has a constant angular velocity where the speed is saturated. In addition, the angular acceleration profile must contain three regions: acceleration, dwell, and deceleration. In general, the acceleration and deceleration regions have the same shape but opposite sign. Therefore, only the acceleration region needs to be designed, and the other regions then can be generated naturally.

The angular acceleration function in the acceleration region can be chosen as an arbitrary function, denoted by $a_{ac}(t)$. The goal is to pick a suitable $a_{ac}(t)$ that minimizes the magnitude of the angular acceleration and the magnitude of the residual vibration surrounding the system resonant frequencies. To minimize the magnitude of the angular acceleration, we will minimize the squared magnitude of the difference between the angular acceleration and its mean value. Therefore, the performance to be minimized is

$$J = \frac{1}{2}\int_0^{t_{ac}}\left(a_{ac}(t) - \frac{1}{t_{ac}}\int_0^{t_{ac}} a_{ac}(t)\,dt\right)^2 dt \tag{18}$$

where t_{ac} is the duration of the acceleration region.

To minimize the magnitude of the residual vibration considering frequency uncertainties, we set the magnitude of the residual vibration surrounding the system resonant frequencies κ_j equal to zero. The zero-vibration points can be chosen as in the following equation

$$V\left(\kappa_{\min j} + \frac{i\left(\kappa_{\max j} - \kappa_{\min j}\right)}{n_j - 1}\right) = 0 \tag{19}$$

where $\kappa_{\min j}$ and $\kappa_{\max j}$, which are symmetrical about κ_j, represent the minimum and maximum zero-vibration points around κ_j, respectively, and

$$i = 0, 1, \cdots, n_j - 1 \tag{20}$$

where n_j, which is an integer greater than 1, represents the number of zero-vibration points around κ_j.

Generally, the upper and lower bounds of κ_j are symmetrical about κ_j. To describe them uniformly, the *Uncertainty Ratio* of the j^{th} mode is defined as

$$\beta_j = \frac{\kappa_j - \kappa_{Lj}}{\kappa_j} = \frac{\kappa_{Uj} - \kappa_j}{\kappa_j} \tag{21}$$

where β_j is the uncertainty ratio of the j^{th} mode, κ_{Uj} is the upper bound of κ_j, and κ_{Lj} is the lower bound of κ_j. The relationships among κ_{Uj}, κ_{Lj}, $\kappa_{\max j}$, $\kappa_{\min j}$ and κ_{ij} are shown in Fig. 1

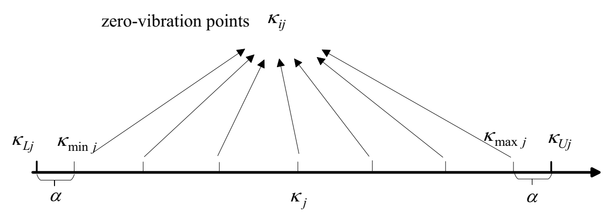

Fig. 1. Frequency bounds and zero-vibration points

To simplify Eq. (19), we define

$$\kappa_{ij} = \kappa_{\min j} + \frac{i\left(\kappa_{\max j} - \kappa_{\min j}\right)}{n_j - 1} \tag{22}$$

where κ_{ij} represents the ith zero point around the jth mode frequency κ_j.

With Eq. (17), Eq. (19) can be written as the following $\sum_{j=1}^{m} n_j$ equations:

$$\int_0^{t_{ac}} a_{ac}(t)\,e^{\kappa_{ij}\xi t}\cos\left(\kappa_{ij}\sqrt{1-\xi^2}t\right)dt = 0, \text{ and} \tag{23}$$

$$\int_0^{t_{ac}} a_{ac}(t)\,e^{\kappa_{ij}\xi t}\sin\left(\kappa_{ij}\sqrt{1-\xi^2}t\right)dt = 0 \tag{24}$$

where $j = 1, 2, \cdots, m$. To ensure the angular rate at the end of the acceleration equals the maximum angular rate, the following constraint should be added

$$\omega_{\max} = \int_0^{t_{ac}} a_{\text{ac}}(t)\,dt \tag{25}$$

where $\omega_{\max}$ is the maximum angular rate.

Substituting Eq. (25) into Eq. (18), the performance J can be simplified as

$$J=\frac{1}{2}\int_0^{t_{ac}}\left(a_{ac}\left(t\right)-\frac{\omega_{\max}}{t_{ac}}\right)^2dt \tag{26}$$

Based on the principle of the calculus of variations, to minimize the performance index, Eq. (26) subject to the constraints of Eq. (23), Eq. (24) and Eq. (25), the following Euler-Lagrange equation should be satisfied:

$$\frac{\partial L}{\partial a_{ac}}-\frac{d}{dt}\left(\frac{\partial L}{\partial \dot{a}_{ac}}\right)=0 \tag{27}$$

where L is the Lagrangian, which is expressed as

$$\begin{aligned}L=&\frac{1}{2}\left(a_{ac}\left(t\right)-\frac{\omega_{\max}}{t_{ac}}\right)^2+\lambda a_{ac}\left(t\right)\\&+\sum_{j=1}^{m}\sum_{i=1}^{n_j}\left(\lambda_{cij}a_{ac}\left(t\right)e^{\kappa_{ij}\xi t}\cos\left(\kappa_{ij}\sqrt{1-\xi^2}t\right)\right)\\&+\sum_{j=1}^{m}\sum_{i=1}^{n_j}\left(\lambda_{sij}a_{ac}\left(t\right)e^{\kappa_{ij}\xi t}\sin\left(\kappa_{ij}\sqrt{1-\xi^2}t\right)\right)\end{aligned} \tag{28}$$

where λ, λ_{cij} and λ_{sij} are constant co-state variables.

Substituting Eq. (28) into Eq. (27), the optimal expression of $a_{\mathrm{ac}}\left(t\right)$ is obtained as

$$\begin{aligned}a_{ac}\left(t\right)=&\frac{\omega_{\max}}{t_{ac}}-\lambda\\&-\sum_{j=1}^{m}\sum_{i=1}^{n_j}\lambda_{cij}e^{\kappa_{ij}\xi t}\cos\left(\kappa_{ij}\sqrt{1-\xi^2}t\right)\\&+\sum_{j=1}^{m}\sum_{i=1}^{n_j}\lambda_{sij}e^{\kappa_{ij}\xi t}\sin\left(\kappa_{ij}\sqrt{1-\xi^2}t\right)\end{aligned} \tag{29}$$

The expression for $a_{\mathrm{ac}}\left(t\right)$ was then obtained as shown in Eq. (29), but there are $1+\sum_{j=1}^{m}n_j$ unknown constants λ, λ_{cij} and λ_{sij}. The next step is to determine the unknown constants using the constraint equations Eq. (23), Eq. (24) and Eq. (25). First, substituting Eq. (29) into Eq. (23), Eq. (24) and Eq. (25), a group of linear equations of $1+\sum_{j=1}^{m}n_j$ dimensions is then obtained as Eq. (33), where $l\in\mathbb{N}^+$ vary from 1 to m, $k\in\mathbb{N}^+$ vary from 1 to n_l, and c_{ij}, s_{ij}, C_{ijkl}, M_{ijkl}, N_{ijkl} and S_{ijkl} are constants that can be calculated by Eq. (34).

The analytical expressions for c_{ij}, s_{ij}, C_{ijkl}, M_{ijkl}, N_{ijkl}, S_{ijkl} can be derived from a simple knowledge of calculus. The unknown variables λ, λ_{cij} and λ_{sij} can be uniquely obtained by solving the linear equations of E-q. (33). The derivation of the optimal angular acceleration profile is now finished. In Eq. (29), the variables t_{ac}, κ_{minj}, and κ_{maxj} should be assigned in advance to ensure that the amplitude of the angular acceleration and the residual vibration ratio satisfy the following constraints:

$$\max(a_{ac}(t))\leq a_{\max},\ \text{and} \tag{30}$$

$$\max\left(\upsilon\left(\kappa\right)\right)\leq\upsilon_{\max},\quad \kappa\in\bigcup\nolimits_{j=1}^{m}\left[\kappa_{Lj}\ \kappa_{Uj}\right] \tag{31}$$

where $a_{\max}$ represents the maximum allowed angular acceleration, and $\upsilon_{\max}$ represents the maximum allowed residual vibration ratio. To describe the changes in κ_{minj} and κ_{maxj}, we define a variable α_j expressed as

$$\alpha_j=\kappa_{minj}-\kappa_{Lj}=\kappa_{Uj}-\kappa_{maxj} \tag{32}$$

The α_j can be suitably and simply selected by setting them to the same value denoted by α in Fig. 1, which means the following equation holds:

$$\alpha=\alpha_1=\alpha_1=\cdots=\alpha_m \tag{35}$$

Then, $\max(a_{ac}(t))$ and $\max\left(\upsilon\left(\kappa\right)\right)$ are determined u-niquely by t_{ac} and α. With certain n_j, κ_j and β, the relationship between t_{ac}, α and $\max(a_{ac}(t))$ and the relationship between t_{ac}, α and $\max\left(\upsilon\left(\kappa\right)\right)$ can be obtained. These relationships can be visualized via a contour line, and then optimal t_{ac} and α can be found to keep both the angular acceleration and residual vibration within acceptable bounds, at the same time, to minimize the acceleration time.

The following is a example. The parameters are $\kappa_1=1\mathrm{rad/s}$, $\zeta=0$, and $\beta=0.36$, $a_{\max}=0.003\mathrm{rad/s}^2$ and $\upsilon_{\max}=0.05$. The contour line of $\max(a_{ac}(t))$ and $\max\left(\upsilon\left(\kappa\right)\right)$ with $n_1=3$, $n_1=4$ and $n_1=5$ are then shown in Figs. 2, 3 and 4, respectively. The the horizontal ordinate of these figures is α, the vertical ordinate is acceleration time, and the counter line represents the maximum acceleration and maximum residual vibration ratio respectively.

Under the constraints of Eq. (30) and Eq. (31), the values of t_{ac} and α corresponding to the minimum acceleration time are

$$\left\{\begin{array}{lll}t_{ac}=14.5\mathrm{s},\alpha=0.043 & \text{for} & n_1=3\\ t_{ac}=13.9\mathrm{s},\alpha=0.025 & \text{for} & n_1=4\\ t_{ac}=16.5\mathrm{s},\alpha=0.02 & \text{for} & n_1=5\end{array}\right. \tag{36}$$

In these three groups of values, the acceleration time of $n_1=4$ is a minimum, the values of t_{ac}, α and n_1 were therefore chosen to be $t_{ac}=13.9\mathrm{s},\alpha=0.025$ and $n_1=4$. The corresponding acceleration curve and residual vibration ratio are shown in Fig. 5.

From these figures, we can summarize an approximation law: fix t_{ac}, and $\max(a_{ac}(t))$ will increase approximately with the increase in n_j, but $\max\left(\upsilon\left(\kappa\right)\right)$ will decrease approximately with the increase in n_j. Therefore, if the constraints shown in Eq. (30) and Eq. (31) are not satisfied, we can adjust n_j according to this law. In addition, from Fig. 5 we found an interesting law: if $\xi=0$ the angular acceleration in the acceleration region will be symmetrical about line $t=\frac{t_{ac}}{2}$. This law is generally true with other simulations, but it is difficult to prove.

To obtain the integrated angular acceleration profile, the dwell time, which is denoted t_{dwell}, should be calculated first. t_{dwell} can be calculated by the following steps. The maneuver Euler angle, Φ_f, can be expressed as

$$\Phi_f=\Phi_{ac}+\Phi_{dwell}+\Phi_{dec} \tag{37}$$

where Φ_{ac} is the rotation angle in the acceleration region, Φ_{dwell} is the rotation angle in the dwell region, and

$$\begin{cases} -\lambda t_{ac} - \sum_{j=1}^{m}\sum_{i=1}^{n_j}\lambda_{cij}c_{ij} - \sum_{j=1}^{m}\sum_{i=1}^{n_j}\lambda_{sij}s_{ij} = 0 \\ \left(\frac{\omega_{\max}}{t_{ac}} - \lambda\right)c_{kl} - \sum_{j=1}^{m}\sum_{i=1}^{n_j}\lambda_{cij}C_{ijkl} - \sum_{j=1}^{m}\sum_{i=1}^{n_j}\lambda_{sij}M_{ijkl} = 0 \\ \left(\frac{\omega_{\max}}{t_{ac}} - \lambda\right)s_{kl} - \sum_{j=1}^{m}\sum_{i=1}^{n_j}\lambda_{cij}N_{ijkl} - \sum_{j=1}^{m}\sum_{i=1}^{n_j}\lambda_{sij}S_{ijkl} = 0 \end{cases} \tag{33}$$

$$\begin{aligned} c_{ij} &= \int_0^{t_{ac}} e^{\kappa_{ij}\xi t}\cos\left(\kappa_{ij}\sqrt{1-\xi^2}t\right)dt \\ s_{ij} &= \int_0^{t_{ac}} e^{\kappa_{ij}\xi t}\sin\left(\kappa_{ij}\sqrt{1-\xi^2}t\right)dt \\ C_{ijkl} &= \int_0^{t_{ac}} e^{\kappa_{ij}\xi t}e^{\kappa_{kl}\xi t}\cos\left(\kappa_{ij}\sqrt{1-\xi^2}t\right)\cos\left(\kappa_{kl}\sqrt{1-\xi^2}t\right)dt \\ M_{ijkl} &= \int_0^{t_{ac}} e^{\kappa_{ij}\xi t}e^{\kappa_{kl}\xi t}\sin\left(\kappa_{ij}\sqrt{1-\xi^2}t\right)\cos\left(\kappa_{kl}\sqrt{1-\xi^2}t\right)dt \\ N_{ijkl} &= \int_0^{t_{ac}} e^{\kappa_{ij}\xi t}e^{\kappa_{kl}\xi t}\cos\left(\kappa_{ij}\sqrt{1-\xi^2}t\right)\sin\left(\kappa_{kl}\sqrt{1-\xi^2}t\right)dt \\ S_{ijkl} &= \int_0^{t_{ac}} e^{\kappa_{ij}\xi t}e^{\kappa_{kl}\xi t}\sin\left(\kappa_{ij}\sqrt{1-\xi^2}t\right)\sin\left(\kappa_{kl}\sqrt{1-\xi^2}t\right)dt \end{aligned} \tag{34}$$

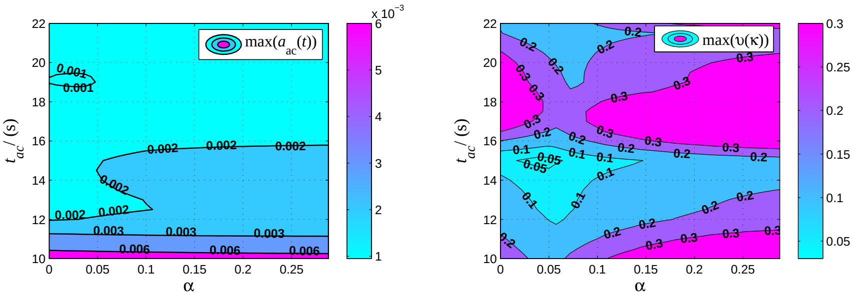

(a) (b)

Fig. 2. Contour line with $n_1 = 3$: a) Maximum amplitude of the angular acceleration profile b) Maximum residual vibration ratio

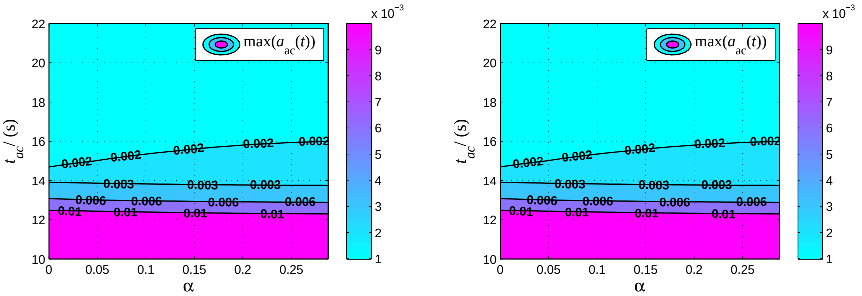

(a) (b)

Fig. 3. Contour line with $n_1 = 4$: a) Maximum amplitude of the angular acceleration profile b) Maximum residual vibration ratio

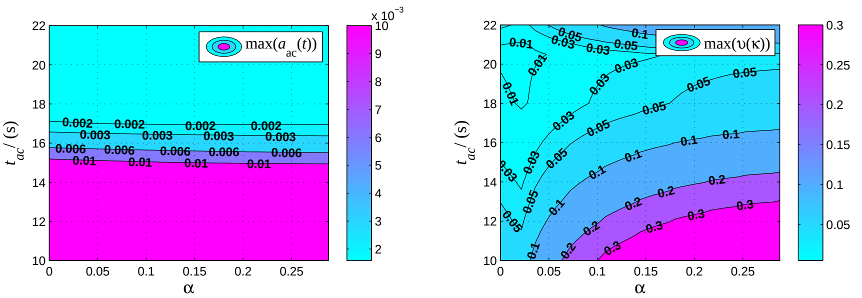

(a) (b)

Fig. 4. Contour line with $n_1 = 5$: a) Maximum amplitude of the angular acceleration profile b) Maximum residual vibration ratio

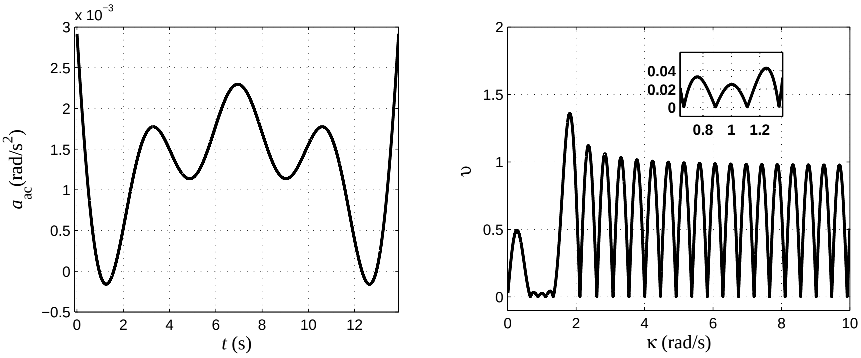

(a) (b)

Fig. 5. Shaped angular acceleration profile and residual vibration ratio with $n_1 = 4$: a) Shaped angular acceleration profile b)Residual vibration ratio

Φ_{dec} is the rotation angle in the deceleration region. The expression for Φ_{ac}, Φ_{dwell}, and Φ_{dec}, which are shown in Fig. 6, are

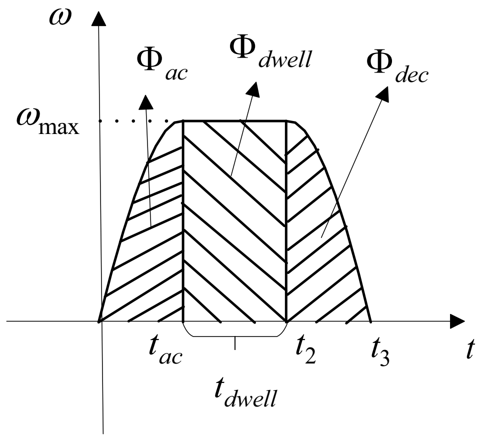

Fig. 6. Relationship of maneuver parameters

$$\Phi_{ac} = \int_0^{t_{ac}} \left(\int_0^t a_{ac}(\tau) d\tau \right) dt, \tag{38}$$

$$\Phi_{dwell} = \omega_{\max} t_{dwell}, \text{ and} \tag{39}$$

$$\begin{aligned} \Phi_{dec} &= \textstyle\int_{t_2}^{t_3} \left(\omega_{\max} - \int_{t_2}^{t} a_{ac}(\tau - t_2) d\tau \right) dt \\ &= \omega_{\max} t_{ac} - \textstyle\int_0^{t_{ac}} \left(\int_0^t a_{ac}(\tau) d\tau \right) dt \end{aligned} \tag{40}$$

where

$$t_2 = t_{ac} + t_{dwell}, \text{ and} \tag{41}$$

$$t_3 = 2t_{ac} + t_{dwell} \tag{42}$$

After substituting Eq. (38), Eq. (39), and Eq. (40) into Eq. (37), simplifying yields

$$t_{dwell} = \frac{\Phi_f}{\omega_{\max}} - t_{ac} \tag{43}$$

To reduce the maneuver time, $\omega_{\max}$ should be chosen to be as large as possible under the constraint of the actuator capability. However, t_{dwell} must equal or be greater than 0, and the following constraint should therefore be satisfied:

$$\Phi_f \geq \omega_{\max} t_{ac} \tag{44}$$

IV. Simulations

This section presents a group of simulations to verify that the designed angular acceleration profile can reduce the residual vibration effectively with frequency uncertainty.

A. Simulation Description

The simulation parameters are presented in Table. I. The lower and upper bounds of the natural frequencies can be calculated as follows: $\kappa_{L1} = 0.64$rad/s, $\kappa_{U1} = 1.36$rad/s, $\kappa_{L2} = 3.2$rad/s, and $\kappa_{U2} = 6.8$rad/s. In the simulation, the actual frequencies are selected as their lower bounds, which are 0.64 rad/s and 3.2 rad/s respectively.

TABLE I
Satellite parameters

Parameter	Value
$\boldsymbol{I}$	$\begin{bmatrix} 500 & -20 & 13 \\ -20 & 500 & 32 \\ 13 & 32 & 500 \end{bmatrix}$ kg · m²
$\boldsymbol{\Omega}$	diag([1 5]) rad/s
$\boldsymbol{B}$	$\begin{bmatrix} 1.1 & -2.2 & 0 \\ -1.6 & -10.7 & -2.3 \end{bmatrix}^{\mathrm{T}}$
ξ	0.01
β	36%
k_p	0.0016
k_d	0.072
$a_{\max}$	0.003 rad/s²
$\upsilon_{\max}$	0.05
$\omega_{\max}$	0.175 rad/s
Φ_f	1 rad

Considering the actuator capacity, the amplitude of the angular acceleration should satisfy the following requirement:

$$\max\left(a_{\mathrm{ac}}\left(t\right)\right) \leq a_{\max} \qquad t \in [0 \quad t_{ac}] \tag{45}$$

In addition, to reduce residual vibrations surrounding the natural frequencies, the maximum amplitude of the residual vibration ratio should satisfy the following requirement:

$$\max(\upsilon\left(\kappa\right)) < \upsilon_{\max} \quad \kappa \in [\kappa_{L1} \quad \kappa_{U1}] \cup [\kappa_{L2} \quad \kappa_{U2}] \tag{46}$$

The optimal values of n_1 and n_2 were chosen as $n_1 = 4$ and $n_2 = 14$, which correspond to the minimum acceleration time. Actually, the contour lines of $\max(a_{ac}(t))$ and $\max(\upsilon(\kappa))$ for all possible sets of n_1 and n_2 should be given to choose the optimal n_1 and n_2 to minimize the acceleration time under the conditions of Eq. (30) and Eq. (31). However, for simplicity, only the contour lines with optimal n_1 and n_2 are given.

Fig. 7(a) shows the contour lines of $\max(a_{ac}(t))$, and Fig. 7(b) shows the contour lines of $\max(\upsilon(\kappa))$. With the requirements shown in inequalities Eq. (30) and Eq. (31), we found that the minimum t_{ac} is 15.5s, and the corresponding α is 0.025.

According to the parameters chosen in the previous section, the shaped angular acceleration profile is shown in Fig. 8(a), where the maximum amplitude is less than $a_{\max}$, and the corresponding residual vibration ratio is shown in Fig. 8(b), where the residual vibration ratio is less than $\upsilon_{\max}$ in regions $[\kappa_{L1} \quad \kappa_{U1}]$ and $[\kappa_{L2} \quad \kappa_{U2}]$. The requirements of Eq. (40) and Eq. (41) are both satisfied.

For comparison, we designed three sets of simulations with different reference trajectories. The first reference trajectory was generated using a step input of magnitude $a_{\max}$, the second reference trajectory was generated using an s-curve, and the last reference trajectory was generated using the proposed angular acceleration profile. The selection of the s-curve parameters was presented in [9], where the profiles of the angular acceleration and the angular velocity are shown in Fig. 9, where t_a is the unique parameter of s-curve. According to [9], the optimal value of t_a is $\omega_{\max}/a_{\max}$ for this simulation.

The actual frequencies in that set of simulations were set to the lower bounds, [0.64 3.2] rad/s. In addition, the simulation time was 150s, and the maneuver began at 50s.

B. Simulation Results

The integrated shaped angular acceleration profile must contain the acceleration, dwell and deceleration regions. So the shaped angular acceleration profile in the acceleration region must be extended by adding the dwell and deceleration regions. For the shaped angular acceleration profile, the dwell time was determined to be $t_{\mathrm{dwell}} = 41.8$s according to Eq. (43). The integrated acceleration profiles for these three sets of simulations were then obtained and are shown in Fig. 10.

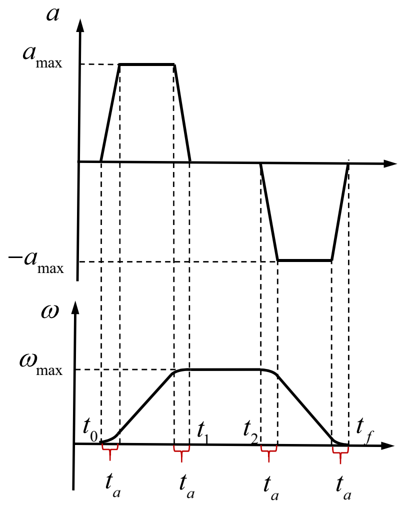

Fig. 9. Angular acceleration and angular velocity of s-curve

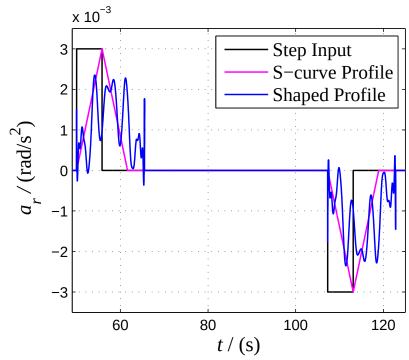

Fig. 10. Integrated angular acceleration profiles

The simulation results are shown in Fig. 11, Fig. 12 and Table. II.

Fig. 11 shows the curve of the residual vibrations. The first-order modal vibrations are shown in Fig. 11(a), where the amplitude of the residual vibration is 0.02 by the excitation of the step input, 0.015 by that of the s-curve input, and 3×10^{-4} by that of the shaped angular acceleration profile. The second-order modal vibrations are shown in Fig. 11(b), where the amplitude of the residual vibration is 2.5×10^{-3} by the excitation of the step input, 1.5×10^{-4} by that of the s-curve input, and 1×10^{-5} by that of the shaped angular acceleration profile. The simulation results shown in Fig. 11 indicate the angular acceleration profile designed by the proposed method can suppress the residual vibration within a certain range. The simulation results also show that the shaped angular acceleration profile has a better vibration suppression effect than the s-curve input, which is because the s-curve input is not suitable for the vibration suppression with a low natural frequency.

The curves for the Euler angle and the projection of angular velocity onto the eigen-axis denoted by ω are shown in Fig. 12. The control errors of the Euler angle shown in Fig. 12(a) are 1×10^{-4}rad, 5×10^{-5}rad, and

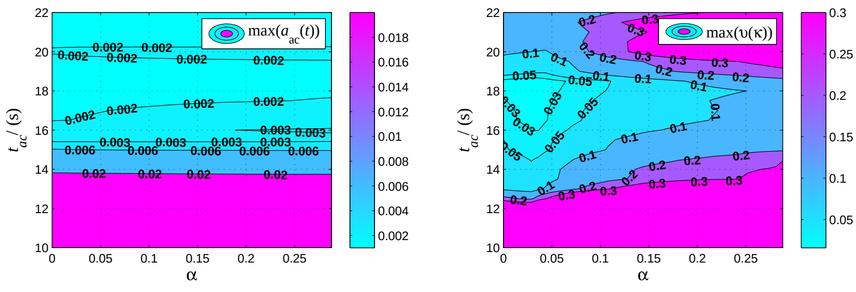

(a) (b)

Fig. 7. Contour lines: a) Maximum amplitude of the angular acceleration profile b) Residual vibration ratio

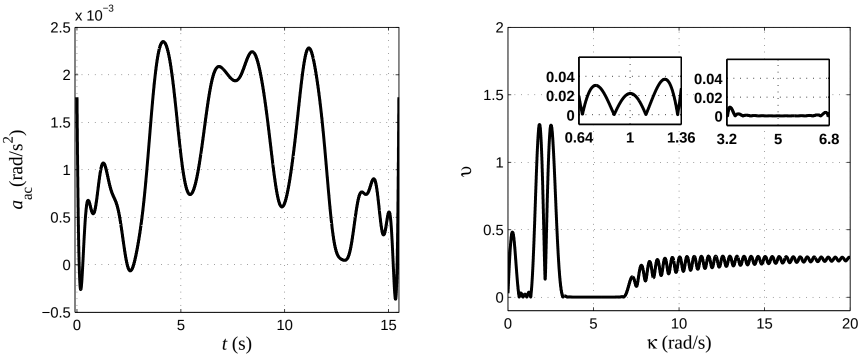

(a) (b)

Fig. 8. Angular acceleration profile and residual vibration ratio a) Angular acceleration profile in the acceleration region b) Residual vibration ratio

TABLE II

SIMULATION RESULTS

Input	Maneuver time (s)	V_1	V_2	Euler angle error (rad)	Angular rate error (rad/s)
Step	100	0.02	2.5×10^{-3}	1×10^{-4}	5×10^{-5}
S-curve	86.5	0.015	1.5×10^{-3}	5×10^{-5}	2×10^{-5}
Shaped profile	72.8	3×10^{-4}	1×10^{-5}	5×10^{-6}	3×10^{-6}

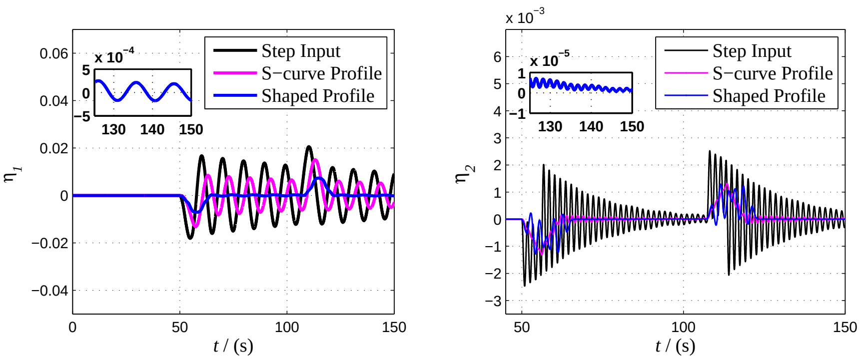

(a) (b)

Fig. 11. Actual modal vibrations: a) First-order natural frequency b) Second-order natural frequency

5×10^{-6}rad using the step input, the s-curve input, and the shaped angular acceleration profile, respectively. The control errors of the angular rate shown in Fig. 12(b) are 5×10^{-5}rad/s, 2×10^{-5}rad, and 3×10^{-6}rad/s using

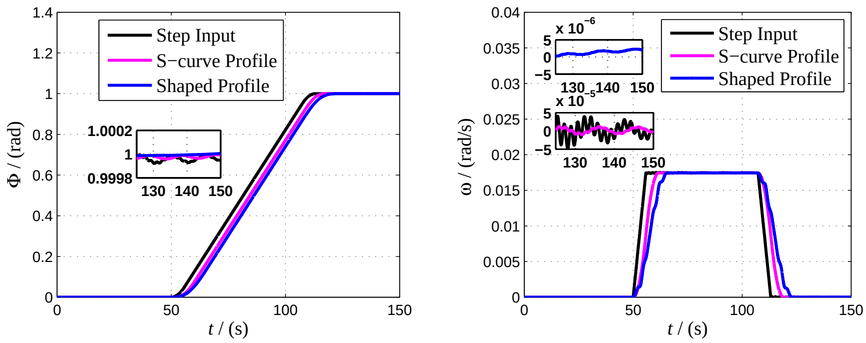

(a) (b)

Fig. 12. Actual attitude and angular velocity: a) Euler angle b) Projection of the angular velocity onto the eigenaxis

the step input, the s-curve input, and the shaped angular acceleration profile, respectively.

For the step input, the absolute value of the eigen-angle and angular velocity were within 1×10^{-4}rad and 1×10^{-5}rad/s after 150s, and the corresponding maneuver time was therefore 100s. For the s-curve input, the absolute value of the eigen-angle and angular velocity were within 1×10^{-4}rad and 2×10^{-5}rad/s after 136.5s, and the corresponding maneuver time was therefore 86.5s. For the shaped angular acceleration profile, the absolute values of the eigen-angle and angular velocity were within 1×10^{-4}rad and 2×10^{-5}rad/s after 122.8s, and the corresponding maneuver time was therefore 72.8s.

Obviously, compared with the step input and the s-curve input, the shaped angular acceleration profile was able to reduce the residual vibrations at the end of the maneuver. Therefore, the maneuver using the shaped input had a higher control precision and shorter maneuver time. In fact, the reference trajectory generated by the step input and the s-curve input had a shorter duration than that generated by the shaped input. However, convergence to a certain control precision requires a long time, which would lead to a longer maneuver time.

V. Conclusions

This paper presents a method for designing reference angular acceleration profiles for flexible satellites to reduce residual vibrations at the ends of maneuvers. An analytical expression for the shaped angular acceleration profiles was obtained to minimize the selected performance. The shaped angular acceleration profiles can be used in a multi-mode system even if the damping ratio is not 0. The simulations show that suitable angular acceleration profiles can be designed using this method, with a consideration of the residual vibration magnitude limit and angular acceleration magnitude limit.

Acknowledgments

Funded under the National Natural Science Foundation of China (61503093, 91438202).

References

[1] Smith, O. J. M., “Posicast control of damped oscillatory systems,” *Proceedings of the IRE*, vol. 45, no. 9, pp. 1249-1255, Jan.-Feb. 1957.

[2] Singer, N. C., and Seering, W. P., “Preshaping command inputs to reduce system vibration,” *Journal of Dynamic Systems, Measurement, and Control*, vol. 112, no. 1, pp. 76-82, Mar. 1990.

[3] Singhose, W. E., Seering, W. P., and Singer, N. C., “Shaping inputs to reduce vibration: a vector diagram approach,” *Proceedings of IEEE International Conference on Robotics and Automation*, Cincinnati, OH, USA, 1990, pp. 922-927.

[4] Singhose, W. E., Seering, W. P., and Singer, N. C., “Residual vibration reduction using vector diagrams to generate shaped inputs,” *Journal of Mechanical Design*, vol. 116, no. 2, pp. 654-659, Jun. 1994.

[5] Singhose, W. E., Derezinski, S., and Singer, N. C., “Extra-insensitive input shapers for controlling flexible spacecraft,” *Journal of Guidance, Control, and Dynamics*, vol. 19, no. 2, pp. 385-391, Mar. 1996.

[6] Singhose, W. E., Seering, W. P., and Singer, N. C., “Input shaping for vibration reduction with specified insensitivity to modeling errors,” *Japan-USA Sym. on Flexible Automation*, Boston, MA, USA, 1996.

[7] Singhose, W. E., “Command shaping for flexible systems: A review of the first 50 years,” *International Journal of Precision Engineering and Manufacturing*, vol. 10, no. 4, pp. 153-168, Otc. 2009.

[8] Singer, N. C., Singhose, W. E., and Seering, W. P., “Comparison of filtering methods for reducing residual vibration,” *European Journal of Control*, vol. 5, no. 2, pp. 208-218, Mar. 1999.

[9] Meckl, P. H., and Arestides, P. B., “Optimized s-curve motion profiles for minimum residual vibration,” *American Control Conference*, Philadelphia, PA, USA, 1998, pp. 2627-2631.

[10] Junkins, J. L., Rahman, Z. H., and Bang, H., “Near-minimum-time control of distributed parameter systems-Analytical and experimental results,” *Journal of Guidance, Control, and Dynamics*, vol. 14, no. 2, pp. 406-415, Mar. 1991.

[11] Swigert, C. J., "Shaped torque techniques," *Journal of Guidance, Control, and Dynamics*, vol. 3, no. 5, pp. 460-467, Sep. 1980.
doi: 10.2514/3.56021

[12] Meckl, P. H., and Seering, W. P., "Controlling velocity-limited systems to reduce residual vibration," *Proceedings of IEEE International Conference on Robotics and Automation*, Philadelphia, PA, USA, 1988, pp. 1428-1433.

[13] Meckl, P. H., and Seering, W. P., "Reducing residual vibration in systems with time-varying resonances," *Proceedings of IEEE International Conference on Robotics and Automation*, Raleigh, NC, USA, 1987, pp. 1690-1695.

[14] Xie, X., Huang, J., and Liang, Z., "Vibration reduction for flexible systems by command smoothing," *Mechanical Systems and Signal Processing*, vol. 39, no. 2, pp. 461-470, Aug. 2013.

HOU Zhili was born in 1989. He received the B. Eng and M. Eng degrees in Aerospace Engineering from the Harbin Institute of Technology, China, in 2011 and 2013 respectively. Now he is a PhD candidate of the Harbin Institute of Technology. And he is doing the internship in Shanghai ASES Spaceflight Technology Co.Ltd. His research interests are rapid attitude maneuver of flexible satellite, flexible satellite vibration suppression, CMG singularity analysis, etc.

Prof. GENG Yunhai was born in 1970. He received the B. Eng degree in Mechanical Engineering from the Tongji University, China, in 1992, and the M. Eng and PhD degrees in Aerospace Engineering from the Harbin Institute of Technology, China, in 1995 and 2003 respectively. Since 2009, he has been the deputy director of Research Centre of Satellite Technology, Harbin, China. He currently teaches and performs researches in the fields of space flight dynamics, aerospace guidance, navigation and control systems.

HUANG Simeng was born in 1991. She received the B. Eng and M. Eng degrees in Aerospace Engineering from the Harbin Institute of Technology, China, in 2014 and 2016 respectively. Now she is a PhD candidate of the Politecnico di Milano, Italy. Her research interests are spacecraft attitude dynamics and control, orbital dynamics and satellite constellation.